processes

Article

Experimental Study on Fracture Toughness of Shale Based on Three-Point Bending Semi-Circular Disk Samples

Jinglin Wen [1], Yongming Yin [1,*] and Mingming Zhang [2]

[1] China Academy of Safety Science and Technology, Beijing 100012, China; wenjl@chinasafety.ac.cn
[2] Sinopec Research Institute of Petroleum Engineering Co., Ltd., SINOPEC, Beijing 100101, China; zhangmm60862.sripe@sinopec.com
[*] Correspondence: syaq_2024@163.com

Abstract: A large number of construction practice projects have found that there are many joints and microcracks in rock, concrete, and other structures, which cause the complexity of rock mechanical properties and are the main cause of geological or engineering disasters such as earthquakes, landslides, and rock bursts. To establish a rock fracture toughness evaluation method and understand the distribution range of fracture toughness of Longmaxi Formation shale, this study prepared three-point bending semi-circular disk shale samples of Longmaxi Formation with different crack inclination angles. The dimensionless fracture parameters of the samples, including the dimensionless stress intensity factors of type I, type II, and T-stress, were calibrated using the finite element method. Then, the peak load of the samples was tested using quasi-static loading, and the load–displacement curve characteristics of Longmaxi Formation shale and the variation in fracture toughness with crack inclination angle were analyzed. The study concluded that the specimens exhibited significant brittle failure characteristics and that the stress intensity factor is not the sole parameter controlling crack propagation in rock materials. With an increase in crack inclination angle, the prefabricated crack propagation gradually transitions from being dominated by type I fracture to type II fracture, and the T-stress changes from negative to positive, gradually increasing its influence on the fracture. An excessively large relative crack length increases the error in fracture toughness test results. Therefore, this paper suggests that the relative crack length a/R should be between 0.2 and 0.6. The fracture load distribution range of shale samples with different crack angles is 3.27 kN to 10.92 kN. As the crack inclination angle increases, the maximum load that the semi-circular disk shale samples can bear gradually increases. The pure type I fracture toughness of Longmaxi Formation shale is 1.13–1.38 MPa·m$^{1/2}$, the pure type II fracture toughness is 0.55–0.62 MPa·m$^{1/2}$, and the T-stress variation range of shale samples with different inclination angles is −0.49–9.48 MPa.

Keywords: three-point bending semi-circular disk; stress intensity factor; T-stress; fracture toughness; shale

Citation: Wen, J.; Yin, Y.; Zhang, M. Experimental Study on Fracture Toughness of Shale Based on Three-Point Bending Semi-Circular Disk Samples. *Processes* **2024**, *12*, 1368. https://doi.org/10.3390/pr12071368

Academic Editor: Zheng Sun

Received: 4 June 2024
Revised: 25 June 2024
Accepted: 27 June 2024
Published: 30 June 2024

1. Introduction

A large body of research has shown that the fracture toughness of rocks has a significant influence on the fracture morphology and initiation pressure of cracks in rocks. Meanwhile, in engineering structures, especially in large-scale engineering structures, the geometric dimensions are increasing, the working environments are becoming more complex, and the functions and purposes are becoming more specialized [1–3]. The integrity and durability of these structures are crucial for ensuring personnel safety and normal operation, carrying significant societal and economic implications. For example, large-scale engineering constructions and mechanical equipment, such as nuclear reactors, offshore drilling platforms, oil and gas pipelines, ships, and warships, are at risk of catastrophic accidents if cracks occur, leading to the destruction or disintegration of rock masses or structures [4]. These issues fall within the realm of fracture mechanics, a field of great importance for preventing such failures. The fracture mechanics parameters of rock materials, such as fracture toughness, significantly impact the rock fragmentation process in engineering problems like petroleum drilling and tunnel excavation. Consequently, the importance of rock fracture toughness is increasingly emphasized in geotechnical and mining engineering. The presence of numerous joints and microcracks in natural or engineering materials, such as rocks and concrete, complicates their mechanical properties and is a major cause of geological or engineering disasters, including earthquakes, collapses, and rock bursts [5,6]. The complex stress state in engineering or deep rock masses, where crack tips are subjected to tensile and shear stresses, often results in I–II mixed-mode fracture. Therefore, research on the fracture toughness and propagation paths of rock cracks with I–II mixed-mode fracture has significant theoretical and engineering significance.

Various geometric configurations of test specimens are used for rock fracture toughness testing, including short rod (SR), chevron-notched three-point bending round bar (SECRBB), chevron-notched three-point bending round bar (CB), straight-through crack Brazilian disk (CSTBD), chevron-notched Brazilian disk (CCNBD), and straight-through notch semi-circular bending (SCB) specimens [7–10]. The International Society for Rock Mechanics (ISRM) has recommended SR, CB, CCNBD, and SCB specimens for type I static fracture toughness testing due to their reliability and consistency across different rock types. Testing methods for rock fracture toughness can be classified by loading methods into direct tensile, compressive, and bending types. Indirect tensile methods, such as disk tests, are particularly popular due to their simplicity and ease of implementation [11–14]. These methods have become standard practice in rock fracture toughness testing, providing valuable insights into the mechanical properties and failure mechanisms of various rock types [15–18]. According to the shape of prefabricated cracks, specimens are divided into chevron-notched, straight-notched, and unnotched types [19]. So far, ISRM has recommended four methods for testing rock type I fracture toughness: chevron-notched three-point bending round bar, chevron-notched short rod, chevron-notched Brazilian disk, and straight-notch three-point bending semi-circular disk specimens [20]. In recent years, straight-notch semi-circular disk three-point bending specimens have gained increasing popularity among rock mechanics researchers both domestically and internationally due to their unique advantages. However, during the test process, the influence of T-stress on fracture toughness and crack initiation angle test results is generally not considered. Li et al. [18] believed that cracks in a state of compressive stress still experience tensile–shear stress at the crack tip, and their experiments found a proportional relationship between type I fracture toughness and compressive strength. Gunsallus [19], Whittaker [20], Bhagat [21], and others [22–25] have identified a proportional relationship between rock type I fracture toughness and tensile strength. However, their work primarily involves data fitting formulas based on statistical methods, with limited theoretical analysis of this relationship. Deng et al. [22] provided a theoretical demonstration of the correlation between rock fracture toughness and tensile strength, explaining that the strong correlation is due to their identical failure mechanisms. Additionally, Zhang [24] found a power function relationship between type I fracture toughness and tensile strength in various rock types. Despite the different factors considered in these studies, the relationship between rock type I fracture toughness and tensile strength still requires further research. Beyond tensile strength, Jianguo Chen et al. [25] discovered that shale fracture toughness is positively correlated with its density and sonic velocity, but negatively correlated with its organic content. Chang et al. [23] used a linear function to fit the relationship between rock type I fracture toughness and its sonic velocity, uniaxial compressive strength, Young's modulus, Poisson's ratio, density, and porosity. The results showed that fracture toughness is best correlated with sonic velocity (R = 0.80). Ren et al. [10] proposed a notched deep beam (NDB) specimen with an aspect ratio of 2.0 for testing rock mixed-mode fracture, and calibrated the crack tip fracture parameters in 2D and 3D using the finite element method. The NDB specimen, combined with a three-point bending test, can test tensile–shear fracture toughness with any degree of load mixing between pure type I and pure type II. Using

CSTBD and SCB specimens, many domestic and foreign scholars [26–30] have conducted extensive mixed-mode fracture tests on rocks, obtaining the crack propagation paths and fracture strengths of different rocks under various loading conditions. The test results were compared in detail with some fracture criteria, further strengthening the application of fracture criteria in rock mechanics. Related results also show that the ratio of type II fracture toughness to type I fracture toughness in rocks is generally less than 1. Compared with the comprehensive understanding of the mixed-mode fracture strength and crack propagation paths in rocks, there is little discussion and research on the fracture surfaces and inherent fracture mechanisms formed under mixed loading by domestic and foreign scholars [31–34]. Traditional solid mechanics assumes that materials are homogeneous, but rocks are typical porous materials with defects such as microscopic cracks and voids of various shapes and sizes [35–38]. At the same time, rocks are also typical crystalline particle materials, where macroscopic fractures originate from microscopic trans-granular, inter-granular, and coupled fracture modes. Because of the microscopic structural characteristics of rock materials, the fracture surfaces formed are not completely smooth, with shallow hills, ravines, etc., always present on the rock fracture surface [39–42]. Therefore, studying the microscopic characteristics of rock fractures helps to understand the microscopic failure mechanisms of rocks. In deep oil and gas extraction and other fields, studying the fracture surfaces formed under mixed loading also helps to understand the coupling mechanisms between fluids and solid fracture surfaces during fracturing [39,43]. Additionally, Xie et al. [40] believe that the irregularity of rock fracture surfaces also affects the fracture toughness of rocks. Therefore, it is necessary to meticulously characterize the rock fracture surfaces formed under mixed loading. Lin et al. [43] used scanning electron microscopy at 1000× magnification on a micron scale to study the rough surfaces formed by mixed-mode fracture in CSTBD specimens of limestone, finding that the load mixing degree influences the morphological characteristics of rock fracture surfaces at microscopic dimensions. Ren et al. [10] used the maximum shear stress criterion, minimum strain energy density factor criterion, maximum energy release rate criterion, and improved R criterion to predict the mixed-mode fracture strength of sandstone, studying the intrinsic fracture mechanisms of rocks under mixed loading. The results show that the crack propagation paths and fracture toughness predicted by the improved R criterion are closest to the actual experimental values, with a good match between predicted and experimental fracture surfaces. Su et al. [26] compared the engineering applicability of different criteria in terms of cracking angle, critical load, and mixed fracture toughness, showing that the von Mises stress-based mixed fracture criterion is more advantageous for evaluating structural bearing capacity. Tong et al. [27] used finite fracture mechanics theory, coupling energy and stress, to study the failure load of cracks at arbitrary angles, achieving more accurate predictions. Based on the linear elastic mechanics solution of the crack tip stress field, R.G. Irwin [41] first proposed the concept of the stress intensity factor to characterize stress concentration at the crack tip. Many scholars have conducted extensive theoretical and experimental research on the crack tip stress field using the dynamic strength factor. Feng et al. [32] studied the effect of T-stress on the fracture behavior of closed cracks under compression, establishing a theoretical solution for stress near the closed crack tip. Their results showed that under compressive load, stress at the closed crack tip includes both the singular term of the stress intensity factor (K) and the non-singular terms of the three T-stress components (Tx, Ty, and Txy). Theoretical predictions incorporating these T-stress components matched experimental results for sandstone and PMMA specimens. Tang et al. [31] used the maximum tensile strain crack extension criterion considering T-stress to derive formulas for critical water pressure and initial cracking angle, studying factors such as crack inclination, confining pressure, critical crack zone size, T-stress, and Poisson's ratio.

The study of fracture toughness is fundamental to fractured rock mass engineering. Selecting a suitable fracture toughness specimen is crucial for successful experimental research [42,43]. Among various specimens, the semi-circular bend (SCB) specimen has unique advantages: it is easy to process with prefabricated cracks, it allows testing of I–II mixed-mode fracture toughness, it employs a simple three-point bending method, and it is material-efficient. Since Chong and Kuruppu's initial studies [44,45], Ayatollahi and Aliha [2] have used the SCB specimen for rock fracture toughness testing. The International Society for Rock Mechanics [46–48] recommended the SCB specimen for such tests. This study focuses on using the SCB specimen to test the fracture toughness of Longmaxi Formation shale. By analyzing the SCB load curve, obtaining I–II mixed-mode fracture toughness values, and determining the crack initiation angle, this research enhances understanding of the fracability of Longmaxi Formation shale. The findings provide a basis for designing and optimizing fracturing construction schemes.

2. Testing Method and Sample

2.1. Experimental Equipment and Procedure

The experiment utilized an automatic servo material testing machine that independently developed by Southwest Petroleum University, as shown in Figure 1. This apparatus has a maximum normal load capacity of 1200 kN and a stroke length of 100 mm. It is capable of measuring various rock parameters, including uniaxial compressive strength, tensile strength, and hardness.

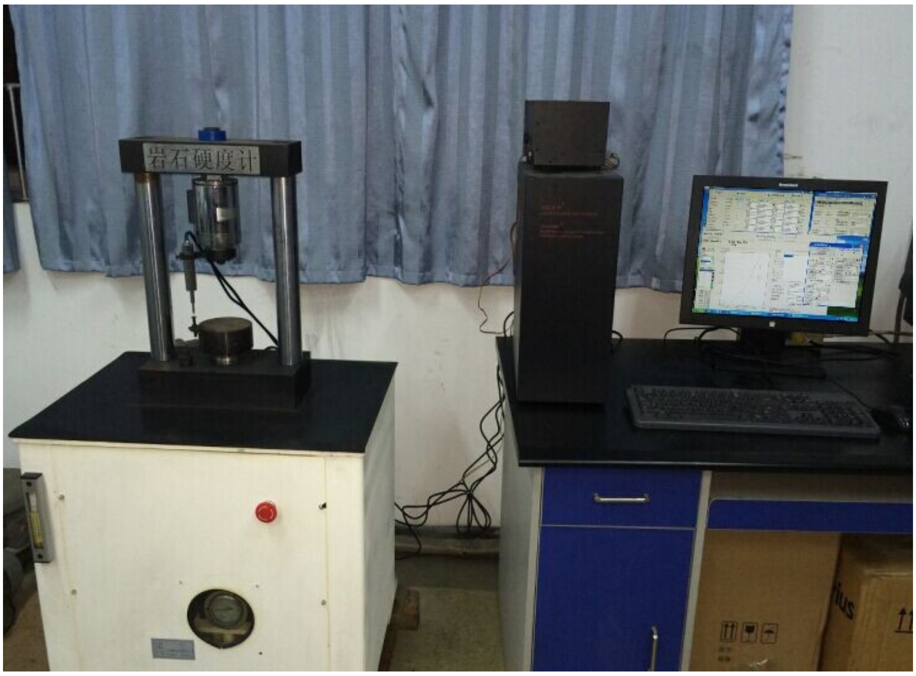

Figure 1. Automatic servo material testing machine.

The experimental loading apparatus and specimens are shown in Figure 2. The requirements for the three-point bending loading apparatus are as follows; firstly, ensure that the loading apparatus makes line contact with the specimen. Secondly, the loading position of the upper indenter should be at the apex of the semi-circular disc. Thirdly, the spacing of the lower support points should be symmetrical around the central axis of the semi-circular disc. Fourthly, the supporting rollers must be aligned in the same plane. Fifthly, the diameter of the rollers should be determined based on the specimen diameter. The ISRM-recommended standard ratio of roller diameter to specimen diameter is 1:20, but the minimum roller diameter should not be less than 5 mm. Sixthly, to ensure quasi-static loading, the loading rate of the indenter on the material testing machine should not exceed 0.2 mm/min.

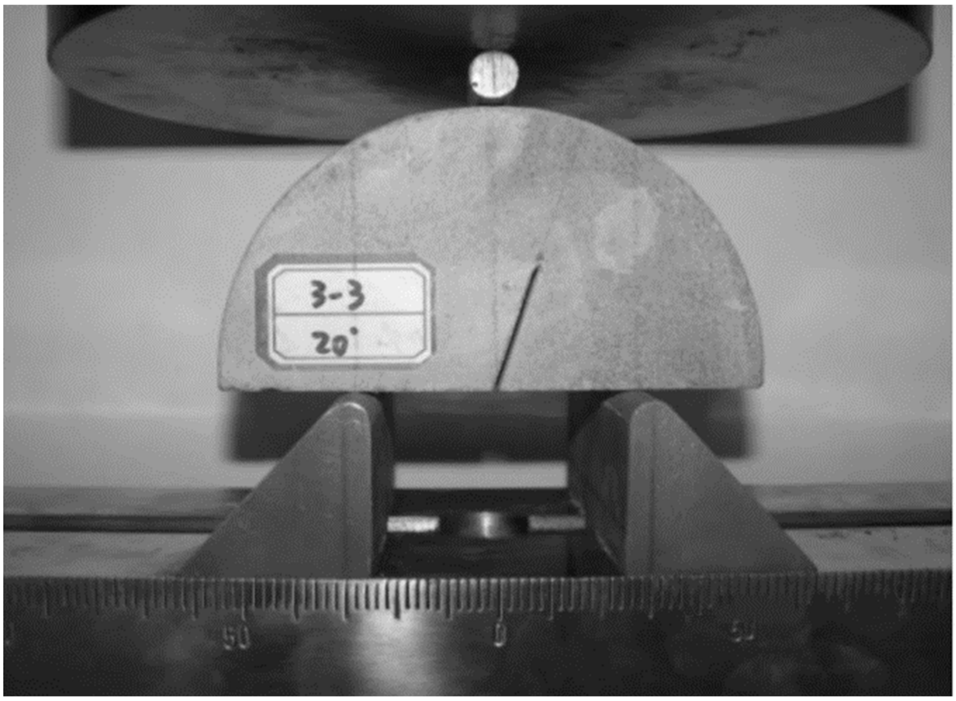

Figure 2. Three-point bending loading device and half-disk specimen.

2.2. Specimen Preparation

Numerous studies by international scholars have demonstrated that the fracture toughness of rock exhibits a size effect, meaning that fracture toughness values for the same rock material can vary depending on the specimen size and type. The ISRM standard [48,49] for testing the fracture toughness of rock specifies several guidelines for the dimensions of semi-circular bend (SCB) specimens. The requirements for standard SCB specimen dimensions are as follows; firstly, the diameter of the semi-circular disc must be at least 10 times the grain size or 76 mm, whichever is greater. Secondly, the thickness must be at least 0.4 times the diameter or 30 mm, whichever is greater. Thirdly, the optimal range for the ratio of the pre-crack length to the radius is between 0.4 and 0.6. Fourthly, the optimal range for the ratio of the support span to twice the radius is between 0.5 and 0.8. Fifthly, the cutting plane should not deviate more than 0.2 mm from the core diameter, and the flatness of the plane should be within 0.5°. Sixthly, the relative pre-crack length should be the average of the measurements obtained on the two flat faces of the semi-disc, and the machining error of the crack length on both faces should be within 2%. Seventhly, the thickness of the specimen must be consistent, with a deviation of no more than 0.2 mm. Eighthly, the measurement errors for the specimen diameter (D), thickness (B), and pre-crack length (a) should be within 0.2 mm. Ninthly, the thickness of the cutting tool should not exceed 0.05 times the diameter (D); otherwise, corrections should be made to the specimen diameter and crack length, as shown in Figure 3. Tenthly, the tensile strength of the material should be measured prior to the fracture toughness test. These specifications ensure the accuracy and reliability of fracture toughness measurements and account for the size effects observed in rock materials.

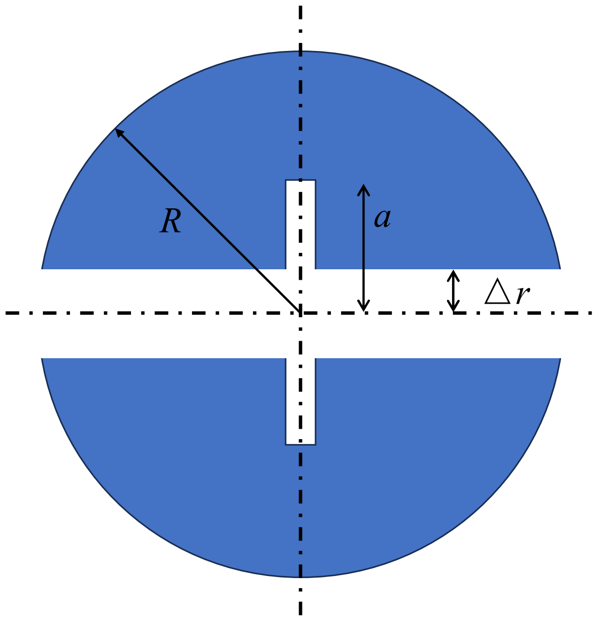

Figure 3. Calibration diagram of half-disk dimensions a and R when the tool thickness cannot be ignored.

In the fracture process of rock materials, a fracture process zone (FPZ) exists. When the radius of this zone is excessively large, it extends beyond the scope of linear elastic fracture mechanics (LEFMs). Therefore, it is crucial to ensure that the SCB specimens are of sufficiently large size so that the dimensions of the FPZ can be considered negligible [48]. This consideration ensures that the assumptions of LEFMs remain valid during testing. Specifically, the SCB specimens should be large enough to contain the FPZ within the linear elastic region, minimizing the influence of the nonlinear processes occurring within the FPZ on the overall fracture toughness measurements. By adhering to this requirement, the validity and reliability of the fracture toughness tests are maintained, providing accurate and meaningful results for engineering applications. Ensuring an adequately sized SCB specimen helps to maintain the integrity of the fracture mechanics analysis and ensures that the test results are representative of the material's true fracture toughness, unaffected by significant nonlinear effects within the FPZ. Chong et al. [45] suggested that the diameter of the SCB specimen should meet the requirement shown in Equation (1):

$$D \geq 2.0\left(\frac{K_{\mathrm{I}c}}{\sigma_{\mathrm{t}}}\right)^2 \quad (1)$$

where σ_{t} represents the tensile strength of the rock, MPa. However, recent studies have shown that the prediction results from the above equation are rather conservative. Currently, the reasonable size of the SCB specimen has not been clearly defined, and the size of the fracture process zone is related to the particle size of the rock material. The ISRM [49] recommends using a certain number of SCB specimens with different diameters to test their fracture toughness, and the diameter of the smallest specimen that remains consistent with the larger size measurement value is considered the reasonable size to ensure effective fracture toughness testing. Taking into account the above requirements, this paper designs the dimensions of the required semi-circular disc specimens as shown in Table 1.

Table 1. Three-point bending half-disk specimen size.

Diameter *D*/mm	Thickness *B*/mm	Support Points Spacing *S*/mm	Crack Length *a*/mm	*B*/*D*	*S*/*R*	*a*/*R*
100	40	60	25	0.4	0.6	0.5

To test the fracture toughness of the rock under mixed-mode I-II loading and fracture angles, as the crack angle increases, the variation of fracture parameters intensifies. To investigate the dominant mode II fracture behavior, cracks were densified within the range of 40° to 50°. Therefore, for this paper, we designed eight semi-circular disc specimens with different crack angles. The specimen model is illustrated in Figure 4.

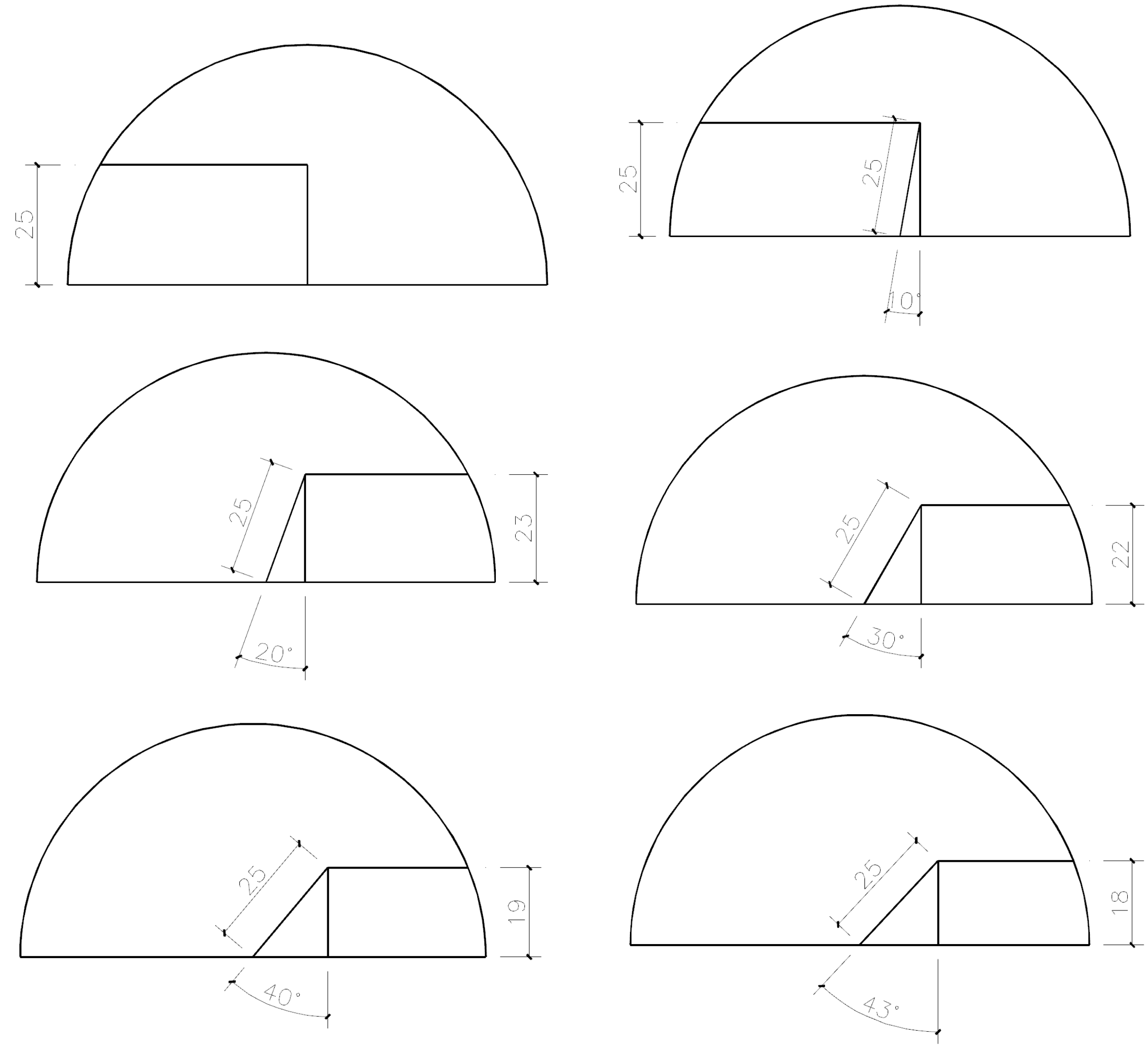

Figure 4. *Cont.*

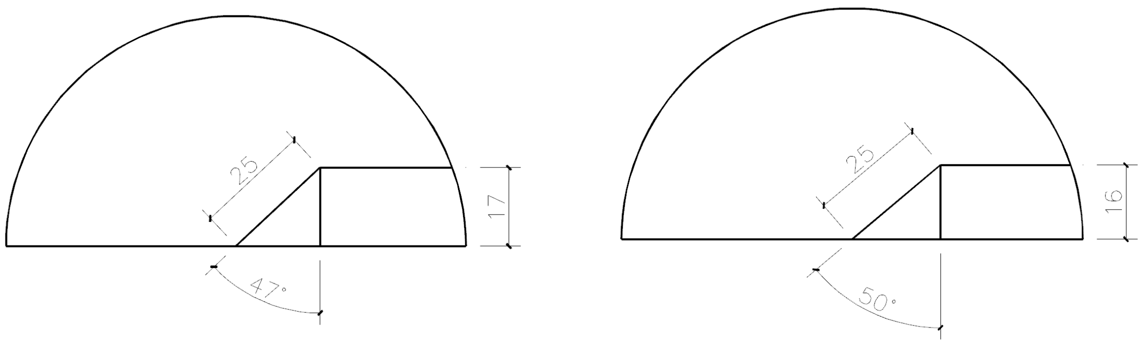

Figure 4. Schematic diagram of composite crack processing for three-point bending half-disk.

The 100 mm diameter cylindrical rock core was cut into two semi-circular discs using a wire saw. After determining the center and crack tip points, an XA5032 vertical milling machine independently developed by Southwest Petroleum University was employed to cut the crack. The tool thickness was 0.4 mm. The process of cutting the crack and the milling machine setup is illustrated in Figure 5.

Figure 5. Semi-disc prefabricated crack processing device.

Shale fracture toughness test specimens with different crack angles were prepared as shown in Figure 6. Semi-circular bend specimens with a relative crack length of 0.5 and crack angles of 0°, 10°, 20°, 30°, 40°, 43°, 47°, and 50° were prepared, with two specimens fabricated for each predetermined crack angle.

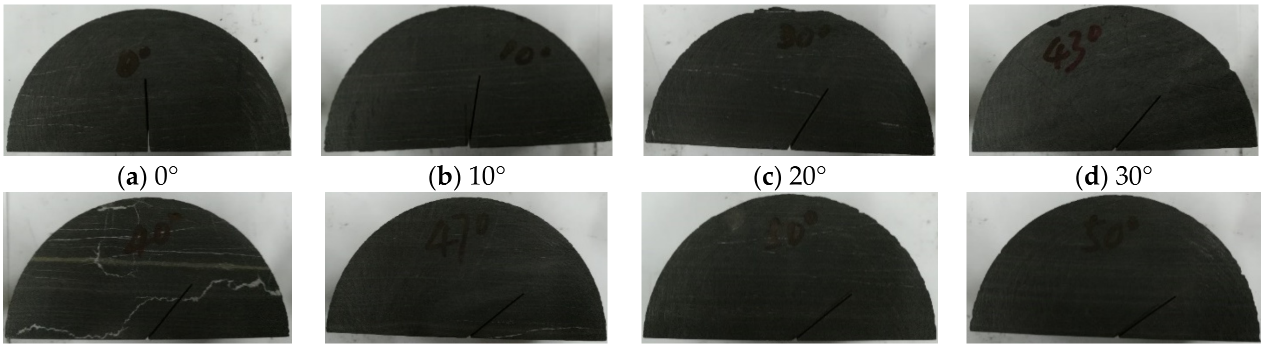

(a) 0° (b) 10° (c) 20° (d) 30°
(e) 40° (f) 43° (g) 47° (h) 50°

Figure 6. Disc shale cores with cracks of different angles.

2.3. Physical Properties of Rock Sample

Ultrasonic transmission testing is a reliable method for studying the mechanical properties of shale rock. It intuitively reflects fundamental physical properties such as mechanical parameters, cementation conditions, porosity, and fractures. In this section, we conduct ultrasonic time-difference tests on cores used for fracture toughness testing to understand and evaluate the characteristics of the cores.

Table 2 presents the P-wave and S-wave transit time parameters for the rock cores used in the fracture toughness test. As shown, the P-wave transit times for shale range from 217.47 μs/m to 288.5 μs/m, while the S-wave transit times range from 342.44 μs/m to 427.02 μs/m.

Table 2. Dimensions and ultrasonic parameters of semi-circular shale specimens for three-point bending.

Pre-Cracked Angle/°	Specimen Diameter *D*/cm	Specimen Thickness *B*/cm	Pre-Cracked Length *a*/mm	P-Wave Transit Time/μs/m	S-Wave Transit Time/μs/m
0	9.95	4.01	25.02	260.71	365.56
	9.96	4.12	25.04	257.17	396.89
10	9.94	4.08	25.01	278.87	427.02
	9.92	4.05	25.12	272.71	388.13
20	9.96	4.01	25.03	273.5	410.46
	9.97	4.03	25.07	274.39	402.53
30	9.98	4.08	25.08	255.19	379.19
	10.51	4.07	25.13	263.21	384.44
43	10.21	4.05	25.12	288.5	420.43
	10.22	4.09	25.04	239.95	379.92
47	9.56	4.11	25.01	225.49	385.38
	9.87	4.08	25.09	229.03	371.97
50	9.94	4.10	25.08	233.26	342.44
	9.74	4.09	25.13	217.47	376.27

This study also included a microscopic examination of the experimental samples using a scanning electron microscope. The microstructure of the shale, as shown in Figure 7, reveals the development of pores and microcracks, with local occurrences of clay minerals and stratification features.

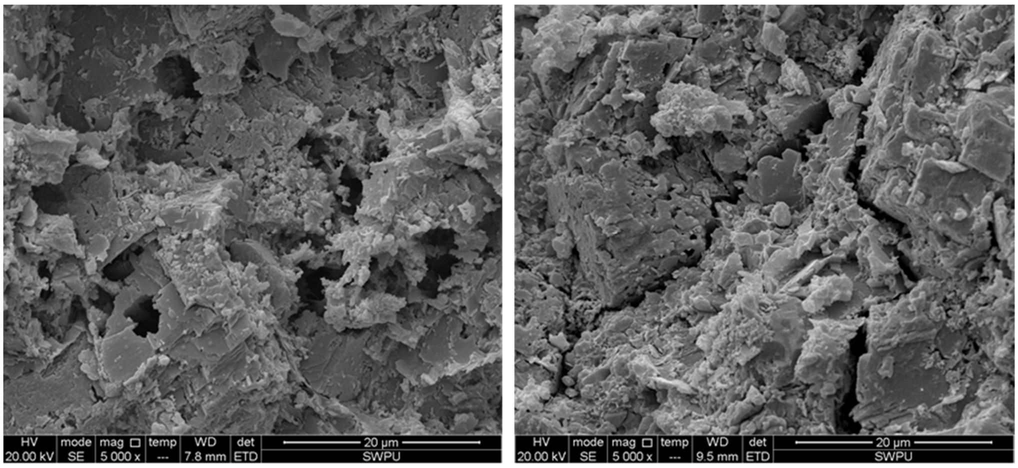

Figure 7. SEM observation images of the microstructure of rock samples.

The physical and mechanical properties of the experimental rock samples were tested and summarized in Table 3. The shale samples used in the experiments had an average density of 2.53 g/cm^3, a porosity of 1.6%, a permeability of 10^{-4} mD, a uniaxial compressive strength of 88.6 MPa, and a tensile strength of 5.8 MPa. Based on the understanding of the basic physical properties of the rock samples, this paper further explores the fracture toughness of shale, as discussed below.

Table 3. Basic physical properties of three-point bending semi-circular shale samples.

Density/(g/cm^3)	**Porosity/%**	**Permeability/mD**	**Uniaxial Compressive Strength/MPa**	**Tensile Strength/MPa**
2.53	1.6	0.0003	88.6	5.8

3. Calibration of Fracture Parameters

The calculation of rock fracture toughness requires the use of maximum load, dimensionless fracture parameters, and specimen dimensions. The dimensionless fracture parameters generally include the mode I dimensionless stress intensity factor, mode II dimensionless stress intensity factor, and dimensionless T-stress. Methods commonly used to determine fracture parameters include analytical methods, numerical analysis methods, and semi-analytical/semi-numerical methods. These parameters are independent of specimen type and are only functions of specimen size and loading conditions. Since there are no analytical results for the dimensionless fracture parameters of the three-point bending semi-circular bend specimens, this study established finite element models of semi-circular bend specimens with different crack lengths and spans to solve for the dimensionless stress intensity factors and T-stress values. The International Society for Rock Mechanics (ISRM) provides a calculation model for the fracture toughness of three-point bending semi-circular bend specimens, as shown in Equations (2)–(4):

$$K_{\mathrm{I}} = \frac{P\sqrt{\pi a}}{2RB} Y_{\mathrm{I}}(a/R, S/2R) \tag{2}$$

$$K_{\mathrm{II}} = \frac{P\sqrt{\pi a}}{2RB} Y_{\mathrm{II}}(a/R, S/2R, \theta) \tag{3}$$

$$T = \frac{P}{2RB} T^{*}(a/R, S/2R, \theta) \tag{4}$$

where P represents the maximum load on the rock fracture test load–displacement curve, kN; K_{I} denotes the rock mode I fracture toughness, MPa·m$^{1/2}$; K_{II} represents the rock mode II fracture toughness, MPa·m$^{1/2}$; T signifies the rock T-stress, MPa; Y_{I}, Y_{II}, and T^*, respectively, denote the dimensionless stress intensity factors for mode I, mode II, and T-stress of the SCB specimen; *R* stands for the radius of the semi-circular bend specimen, mm; *B* represents the thickness of the semi-circular bend specimen, mm; *S* is the distance between the two bottom supports, mm; *a* is the crack length, mm; and α is the inclination angle of the crack.

A finite element model of a three-point bending semi-circular disk was established using ABAQUS 6.14. The material was set to be linear elastic, with an elastic modulus of 4.87 GPa and a Poisson's ratio of 0.388. The analysis assumed a disk diameter of 60 mm, and the model elements were eight-node quadrilateral plane strain elements (CPE8s). A "collapse element" was placed at the crack tip to simulate the stress singularity at the crack tip, with the contour integral radius set to 2 mm and divided into 20 equal parts, as shown in Figure 8.

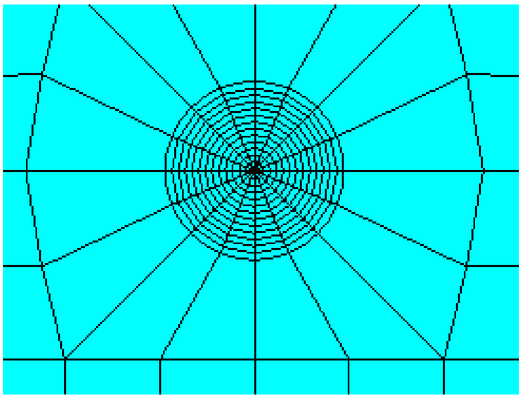

Figure 8. Grid division at the crack tip of SCB specimen.

Theoretically, the J-integral is path-independent, allowing for the selection of any contour path. However, due to stress singularities near the crack tip, integral results close to the crack tip often exhibit significant errors. To improve the accuracy of finite element calculations, this study employed contour paths far from the crack tip. The dimensionless T-stress simulation results for a semi-circular disk with a relative crack length of 0.5 in pure mode I fracture are shown in Figure 9. It can be observed that the integral results for various contour paths are almost identical, ensuring the path independence of the J-integral.

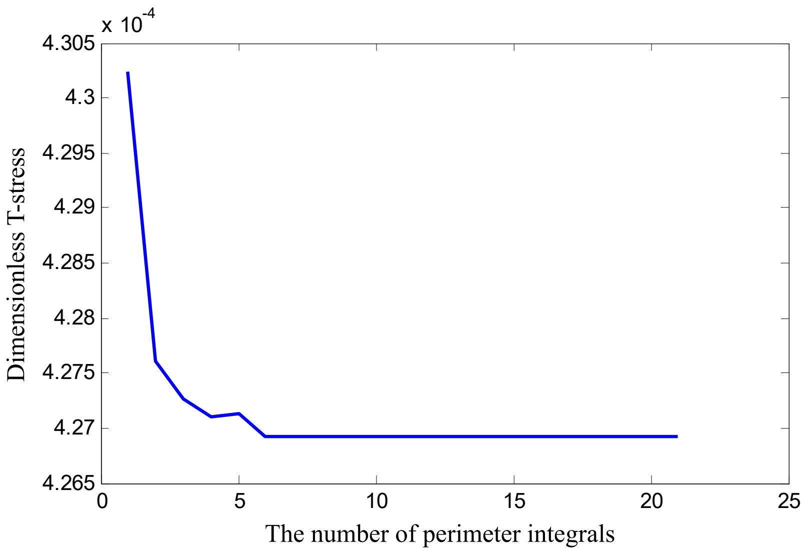

Figure 9. Dimensionless T-stress integral results for SCB under different contour paths.

Based on this model, the stress intensity factor (K) and T-stress were calculated for various crack lengths (a), crack inclinations (θ), and support point distances (S) in the three-point bending semi-circular disk. The dimensionless fracture parameters of the semi-circular bend specimen are calibrated as shown in Table 4 and Figure 10. From Figure 10, it can be observed that the dimensionless stress intensity factor for opening mode Y_{I} decreases gradually as the loading angle increases. The dimensionless stress intensity factor for sliding mode Y_{II} initially increases, and then decreases, with the loading angle, and it approaches 0 when the loading angle is 0. The dimensionless T-stress of the semi-circular bend (SCB) specimen gradually increases as the angle between the applied load and the pre-crack plane increases. When the angle is small, the T-stress is negative and approaches zero. Therefore, in the I–II mixed-mode fracture pattern, where sliding mode fracture predominates, the influence of T-stress on the fracture toughness of rock microcracks and the initiation angle of fractures becomes more significant.

Table 4. SCB specimens with crack length ratio 0.5 and support point spacing ratio 0.6 have no dimensional fracture parameters.

Crack inclination angle α/°	**0**	**5**	**10**	**15**	**20**	**25**	**30**
T^*	−0.46	−0.29	0.18	0.82	1.49	2.10	2.60
Y_{I}	4.58	4.49	4.21	3.80	3.28	2.72	2.15
Y_{II}	0	0.39	0.74	1.01	1.20	1.31	1.34
Crack inclination angle α/°	**35**	**40**	**43**	**47**	**50**	**55**	**60**
T^*	2.98	3.27	3.40	3.55	3.64	3.75	3.82
Y_{I}	1.58	1.05	0.76	0.39	0.15	−0.22	−0.50
Y_{II}	1.31	1.24	1.17	1.06	0.97	0.80	0.60

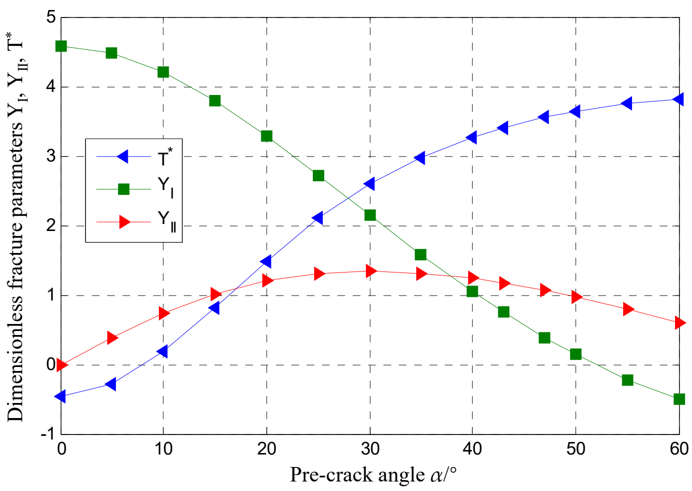

Figure 10. SCB specimens with crack length ratio 0.5 and support point spacing ratio 0.6 have no dimensional fracture parameters.

4. Results and Discussion

4.1. Crack and Load Curve Analysis

To meet the requirements of static loading in rock fracture toughness testing, this study chose displacement-controlled loading to control the loading of the specimen. The loading rate of the material testing machine was set to 0.1 min/mm, allowing for static loading of the load. During the experiment, the static test software automatically collected load data and displayed it in real-time, loading until the rock fractured and stopping loading when the load curve dropped.

Figure 11 shows the fracture paths of shale specimens with different crack angles in the three-point bending semi-circular disk. From the figure, it can be observed that during

Type I fracture, the specimen fractures along the pre-existing crack, forming a through-type straight crack. During Type I–II composite fracture, the specimen initiates from the tip of the pre-existing crack and gradually deviates toward the loading position. Due to natural microcracks, bedding planes, and particle sizes inherent in shale, cracks may deflect during propagation but gradually continue towards the loading position. Figures 12 and 13 display the load–time curves of semi-circular disk shale specimens with different crack angles. The symbol α indicates the inclination of the prefabricated crack in Figures 12 and 13. From these figures, it is evident that the load suddenly drops after rising to a certain height. The load curve exhibits a noticeable nonlinear loading stage, followed by linear loading until the specimen ruptures, causing a sudden and rapid decrease in load.

(**a**) 0° (**b**) 10° (**c**) 20° (**d**) 30° (**e**) 47° (**f**) 50°

Figure 11. Crack propagation path of three-point curved half-disk.

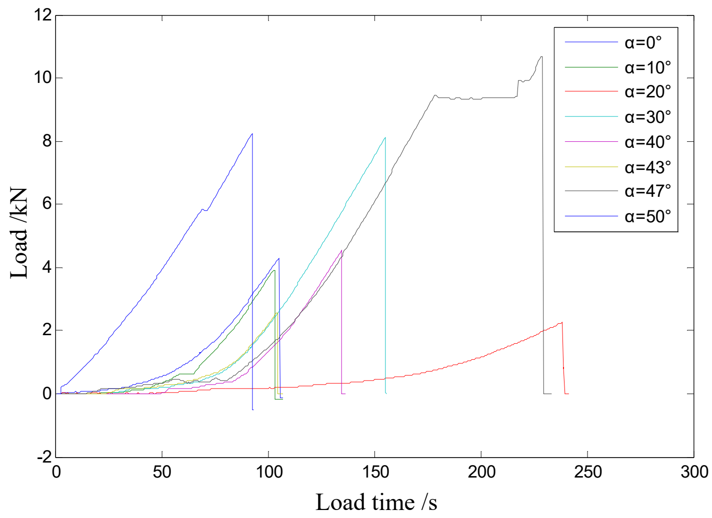

Figure 12. Load–time curve 1 of three-point curved half-disc shale sample.

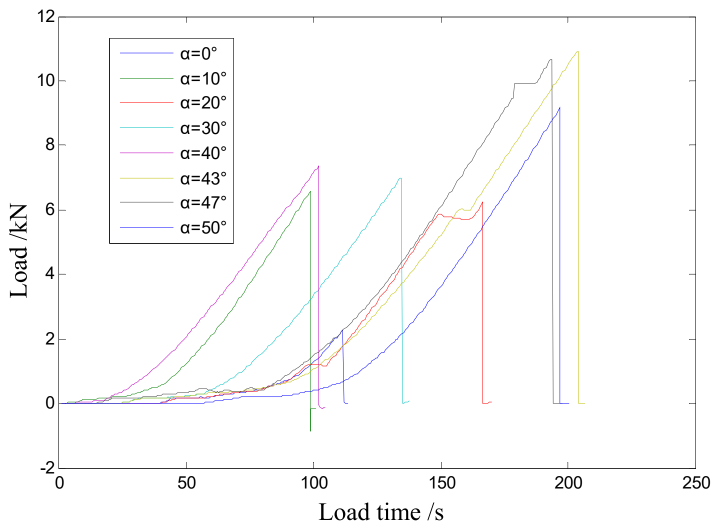

Figure 13. Load–time curve 2 of three-point curved half-disc shale sample.

From the load–time curves of the three-point bending semi-circular disk, it can be observed that each curve undergoes a compacting stage, followed by a sudden failure of the specimen as the load increases. Some shale specimens may spall out, causing a sharp drop in load. The entire process lacks a yielding stage, and the specimens exhibit significant brittle failure characteristics. The initial closure of internal defects within the rock leads to a gradual increase in the slope of the load curve during the early loading stages. Subsequently, the specimens enter a linear elastic stage until brittle failure occurs.

4.2. Fracture Toughness Analysis

Fracture toughness and T stress of the shale samples were calculated using Equations (2)–(4). The angle between the crack initiation direction and the pre-existing crack was measured using a goniometer to obtain the fracture strength and crack initiation angle of the Longmaxi shale samples with different inclination angles, as shown in Table 5.

Table 5. Test results of fracture parameters for SCB with different crack inclination angles.

Crack Angle θ/°	Maximum Load *P*/kN	Mode I Fracture Toughness K_I/MPa·m$^{1/2}$	Mode II Fracture Toughness K_{II}/MPa·m$^{1/2}$	T-Stress/MPa	Crack Initial Angle $-\theta_c$/°
0	4.30	1.38	0.00	−0.49	0
0	3.27	1.13	0.00	−0.26	0
10	3.93	1.16	0.20	0.18	33
10	6.59	1.94	0.34	0.30	35
20	5.29	0.53	0.19	0.85	56
20	6.23	1.43	0.52	2.32	54
30	8.11	1.22	0.76	5.27	57
30	6.98	1.05	0.66	4.54	58
40	4.53	0.33	0.39	3.70	66
40	7.37	0.54	0.64	6.02	67
43	6.56	0.14	0.21	2.18	76
43	10.92	0.58	0.90	9.28	75
47	10.68	0.29	0.79	9.48	79
47	10.67	0.29	0.79	9.47	80
50	9.15	0.10	0.62	8.33	86
50	8.15	0.09	0.55	7.42	85

For shale samples with different crack angles, the range of fracture loads varied from 3.27 kN to 10.92 kN. As the crack angle increased, the maximum load-bearing capacity of the semi-circular shale samples gradually increased. The fracture toughness of Longmaxi shale ranged from 1.13 MPa·m$^{1/2}$ to 1.38 MPa·m$^{1/2}$ for pure mode I fracture, and from 0.55 MPa·m$^{1/2}$ to 0.62 MPa·m$^{1/2}$ for pure mode II fracture. The range of T-stress for shale samples with different crack angles was −0.49 MPa to 9.48 MPa. The variations of fracture toughness (mode I and mode II), T-stress, and pre-existing crack initiation angle with crack inclination angle are plotted in Figures 14–17, respectively. Analysis reveals that the fracture toughness of shale in mode I decreases with an increase in crack inclination angle, while mode II fracture toughness increases with the crack angle. Similarly, T-stress increases with the crack inclination angle, indicating a transition from mode I-dominated fracture to mode II-dominated fracture as the crack angle increases. Moreover, the influence of T-stress increases, with negative T-stress at a crack angle of 0°, suppressing mode I fracture initiation. Additionally, the pre-existing crack initiation angle gradually increases with the crack angle, exhibiting a strong linear relationship between the two factors.

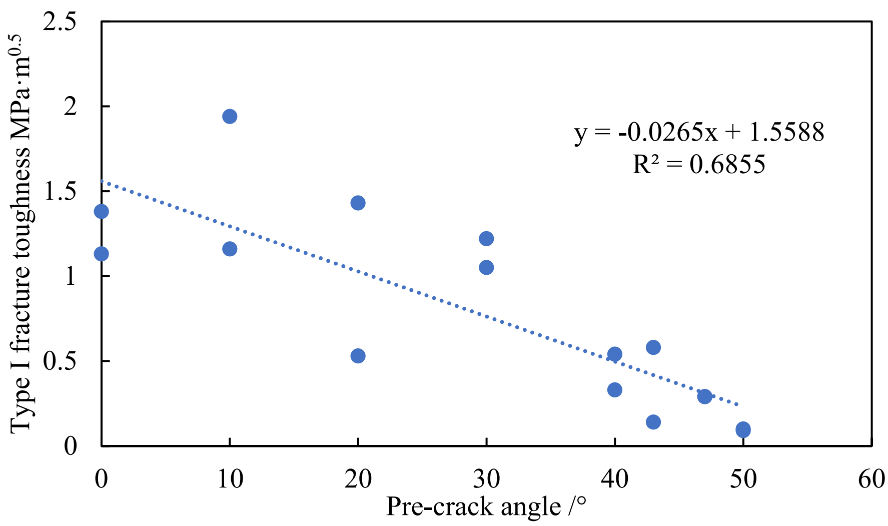

Figure 14. Variation of fracture toughness of mode I with prefabricated crack angle.

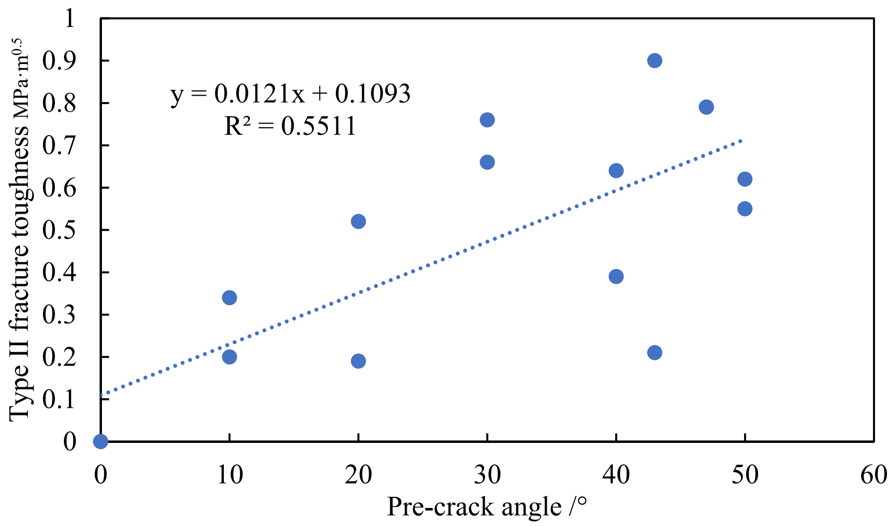

Figure 15. Variation trend of mode II fracture toughness with prefabricated crack inclination.

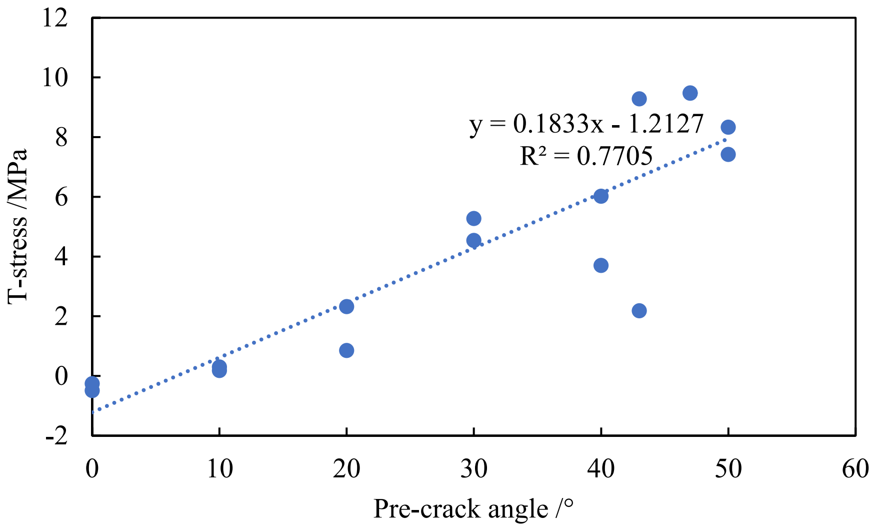

Figure 16. Variation of T-stress at crack tip with prefabricated crack angle.

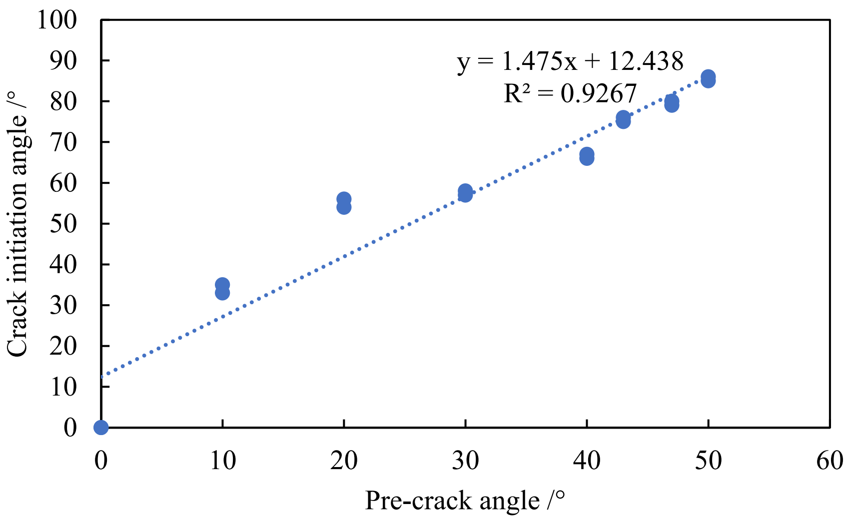

Figure 17. The change in initial crack angle of crack tip with prefabricated crack angle.

5. Conclusions

This study primarily addresses the machining requirements for semi-circular specimen dimensions, the specifications for the three-point bending loading device, and the experimental loading process. Sixteen specimens with eight different crack angles (0°, 10°, 20°, 30°, 40°, 43°, 47°, and 50°) were designed and processed. The fracture parameters of the three-point bending semi-circular specimens, including mode I and mode II dimensionless stress intensity factors and T-stress, were calibrated for various crack angles and support-point distances. The basic physical properties and fracture toughness of Longmaxi shale samples were tested. Through numerical simulation and laboratory experiments, several conclusions were drawn:

(1) The diameter of the semi-circular specimen should be at least 10 times the particle size or 76 mm, with a thickness of at least 0.4 times the diameter or 30 mm. The optimal range for the relative pre-existing crack length a/R is 0.4 to 0.6, and for the relative support point distance $S/2R$, it is 0.5 to 0.8.

(2) The load–time curves of the three-point bending semi-circular specimens all undergo a compaction stage, followed by sudden failure with a sharp drop in load. Some shale specimens may burst out during failure, and the load decreases abruptly. The entire process exhibits significant brittle failure characteristics. The initial closure of internal defects in the rock leads to a gradual increase in the slope of the load curve, followed by entry into the linear elastic stage until brittle failure occurs.

(3) For Longmaxi shale samples with different crack angles, the range of fracture load distribution is 3.27 to 10.92 kN. With an increase in crack angle, the maximum load-bearing capacity of the semi-circular shale specimens gradually increases. The fracture toughness of Longmaxi shale for pure mode I fracture ranges from 1.13 to 1.38 MPa$\cdot$m$^{1/2}$, and for pure mode II fracture, it ranges from 0.55 to 0.62 MPa$\cdot$m$^{1/2}$. The variation range of T-stress for shale samples with different crack angles is -0.49 to 9.48 MPa.

(4) As the inclination angle of the pre-existing crack increases, crack propagation transitions from being controlled by mode I fracture to being dominated by mode II fracture, with the influence of T-stress becoming increasingly significant.

Author Contributions: Conceptualization, J.W.; Software, J.W.; Validation, J.W.; Formal analysis, J.W.; Investigation, Y.Y.; Resources, Y.Y.; Data curation, Y.Y.; Writing—original draft, Y.Y.; Writing—review & editing, M.Z.; Visualization, M.Z.; Supervision, M.Z.; Project administration, M.Z. All authors have read and agreed to the published version of the manuscript.

Funding: This research was funded by National Key Research and Development Program of China (No.2021YFC3001905, 2021YFC3001904, 2021YFC3090403), and Special Funds for Basic Research Business Fees of China Academy of Safety Science and Technology (No.2023JBKY04, 2021JBKY11).

Data Availability Statement: The original contributions presented in the study are included in the article, further inquiries can be directed to the corresponding author.

Conflicts of Interest: Author Mingming Zhang was employed by the company Sinopec Research Institute of Petroleum Engineering Co., Ltd., SINOPEC. The remaining authors declare that the research was conducted in the absence of any commercial or financial relationships that could be construed as a potential conflict of interest. The Sinopec Research Institute of Petroleum Engineering Co., Ltd., SINOPEC had no role in the design of the study; in the collection, analyses, or interpretation of data; in the writing of the manuscript, or in the decision to publish the results.

References

1. Mirsayar, M.M. Mixed mode fracture analysis using extended maximum tangential strain criterion. *Mater. Des.* **2015**, *86*, 941–947. [CrossRef]
2. Aliha, M.R.M.; Ayatollahi, M.R.; Smith, D.J.; Pavier, M.J. Geometry and size effects on fracture trajectory in a limestone rock under mixed mode loading. *Eng. Fract. Mech.* **2010**, *77*, 2200–2212. [CrossRef]
3. Hua, W.; Zhu, Z.; Zhang, W.; Li, J.; Huang, J.; Dong, S. Application of modified fracture criteria incorporating T-stress for various cracked specimens under mixed mode I-II loading. *Theor. Appl. Fract. Mech.* **2024**, *129*, 104184. [CrossRef]

4. Febrian, W.; Nurhalisah, S. Determination of Workload, Work Stress, and Authotarian Leadership Style on Performance Performance. *Dinasti Int. J. Digit. Bus. Manag.* **2024**, *5*, 282–292.
5. Maiti, S.K.; Prasad, K.S.R.K. A study on the theories of unstable crack extension for the prediction of crack trajectories. *Int. J. Solids Struct.* **1980**, *16*, 563–574. [CrossRef]
6. Miao, X.T.; Zhou, C.Y.; Lv, F.; He, X.H. Three-dimensional finite element analyses of T-stress for different experimental specimens. *Theor. Appl. Fract. Mech.* **2017**, *91*, 116–125. [CrossRef]
7. Xie, Y.; Cao, P.; Jin, J.; Wang, M. Mixed mode fracture analysis of semi-circular bend (SCB) specimen: A numerical study based on extended finite element method. *Comput. Geotech.* **2017**, *82*, 157–172. [CrossRef]
8. Dobson, T.; Larrosa, N.; Coules, H. The role of corrosion pit topography on stress concentration. *Eng. Fail. Anal.* **2024**, *157*, 107900. [CrossRef]
9. Gómez-Gamboa, E.; Díaz-Rodríguez, J.G.; Mantilla-Villalobos, J.A.; Bohórquez-Becerra, O.R.; Martínez, M.D.J. Experimental and Numerical Evaluation of Equivalent Stress Intensity Factor Models under Mixed-Mode (I+ II) Loading. *Infrastructures* **2024**, *9*, 45. [CrossRef]
10. Ren, L.; Zhu, Z.; Yang, Q.; Ai, T. Investigation on the applicability of several fracture criteria to the mixed mode brittle fractures. *Adv. Mech. Eng.* **2013**, *5*, 545108. [CrossRef]
11. Khan, S.M.A.; Khraisheh, M.K. A new criterion for mixed mode fracture initiation based on the crack tip plastic core region. *Int. J. Plast.* **2004**, *20*, 55–84. [CrossRef]
12. Subramani, A.; Maimi, P.; Costa, J. On how pseudo-ductility modifies the translaminar fracture toughness of composites and the nominal strength of center-cracked specimens. *Compos. Part A Appl. Sci. Manuf.* **2024**, *184*, 108275. [CrossRef]
13. Li, Y.; Lin, X.; Hu, Y.; Fan, W.; Gao, X.; Yu, J.; Dong, H.; Huang, W. Microstructure and fracture toughness of a Nb–Ti–Si-based in-situ composite fabricated by laser-based directed energy deposition. *Compos. Part B Eng.* **2024**, *278*, 111427. [CrossRef]
14. Cheng, Q.; Huang, G.; Zheng, J.; Liang, Q. New method for determining mode-i static fracture toughness of coal using particles. *Materials* **2024**, *17*, 1765. [CrossRef]
15. Rao, Q.; Sun, Z.; Stephansson, O.; Li, C.; Stillborg, B. Shear fracture (Mode II) of brittle rock. *Int. J. Rock Mech. Min. Sci.* **2003**, *40*, 355–375. [CrossRef]
16. Schmittbuhl, J.; Roux, S.; Berthaud, Y. Development of roughness in crack propagation. *Europhys. Lett.* **1994**, *28*, 585–590. [CrossRef]
17. Backers, T.; Fardin, N.; Dresen, G.; Stephansson, O. Effect of loading rate on Mode I fracture toughness, roughness and micromechanics of sandstone. *Int. J. Rock Mech. Min. Sci.* **2003**, *40*, 425–433. [CrossRef]
18. Li, J.; Gu, D.; Cao, P.; Wu, C. Interrelated law between mode I fracture toughness and compression strength of rock. *J. Cent. South Univ. Sci. Technol.* **2009**, *40*, 1695–1699.
19. Gunsallus, K.L.; Kulhawy, F.H. A comparative evaluation of rock strength measures. *Int. J. Rock Mech. Min. Sci. Geomech. Abstr.* **1984**, *21*, 233–248. [CrossRef]
20. Whittaker, B.N.; Singh, R.N.; Sun, G. *Rock Fracture Mechanics Principles, Design and Applications*; ETDEWEB: Oak Ridge, TN, USA, 1992.
21. Bhagat, R.B. Mode I fracture toughness of coal. *Int. J. Min. Eng.* **1985**, *3*, 229–236. [CrossRef]
22. Deng, H.; Zhu, M.; Li, J.; Wang, Y.; Luo, Q.; Yuan, X. Study of mode I fracture toughness and its correlation with strength parameters of sandstone. *Rock Soil Mech.* **2012**, *33*, 3585–3591. [CrossRef]
23. Chang, S.H.; Lee, C.I.; Jeon, S. Measurement of rock fracture toughness under modes I and II and mixed-mode conditions by using disc-type specimens. *Eng. Geol.* **2002**, *66*, 79–97. [CrossRef]
24. Zhang, Z.X. An empirical relation between mode I fracture toughness and the tensile strength of rock. *Int. J. Rock Mech. Min. Sci.* **2002**, *39*, 401–406. [CrossRef]
25. Chen, J.; Deng, J.; Yuan, J.-L.; Yan, W.; Wei, B.-H.; Tan, Q. Study on evaluation methods of fracture toughness of type I and type II shale reservoirs. *Chin. J. Rock Mech. Eng.* **2015**, *6*, 1101–1105.
26. Su, S.; Cao, S.; Liao, J.; Dong, D. Analysis of I-II Compound Fracture Criteria Based on Apparent Fracture Toughness. *Aeronaut. Sci. Technol.* **2018**, *29*, 67–73. [CrossRef]
27. Tong, G.; Xu, P.; Chen, X. Experimental Study on Three-Point Bending Test of Concrete Specimens with Sharp V-Notch Based on Finite Fracture Mechanics Method. *Exp. Mech.* **2018**, *33*, 253–262.
28. Li, Q.; Yu, Q.; Zhang, S.; Tian, C.; Qian, L.; Li, N. Study on the Strain Gage Test Method of Dynamic Fracture Parameters of Type I Cracks. *J. Rock Mech. Eng.* **2018**, 1430–1437. [CrossRef]
29. Zhao, Y.; Fan, Y.; Zhu, Z.; Zhou, C.; Qiu, H. Theoretical and Experimental Study on the Closure Crack Fracture Behavior under T Stress. *J. Rock Mech. Eng.* **2018**, *37*, 1340–1349.
30. Lv, Y. Experimental Study on Loading Rate Effect of Laminated Shale Fracture Toughness. *J. Rock Mech. Eng.* **2018**, *37*, 1359–1370.
31. Tang, S.; Zhang, H. Research on Rock Fracture Hydraulic Fracturing Based on Maximum Tangential Strain Fracture Criterion. *J. Rock Mech. Eng.* **2016**, 2710–2719. [CrossRef]
32. Feng, R.; Zhu, Z.; Fan, Y. Study on Composite Fracture Properties and Criteria of Sandstone Semi-Circular Bending. *Eng. Sci. Technol.* **2016**, *48*, 121–127.
33. Gao, Y.-H.; Wang, Y.; Cheng, C.-Z. Effect of general T-stress on stress intensity factor of a crack. *J. Univ. Sci. Technol. China* **2009**, *39*, 1319–1322.

34. Hou, C.; Wang, Z.; Wang, Z. Study on Fracture Behavior of Concrete Discs with Centered Straight Cracks Based on Modified Maximum Tangential Stress Criterion. *Sci. China Technol. Sci.* **2016**, *46*, 377–386.
35. Liu, S.; Li, Z. Effect of T stress on critical stress intensity factor of I-II mixed mode crack. *J. Henan Univ. Urban Constr.* **2013**, *22*, 33–37.
36. Wang, Q.Z.; Lei, X. Determination of fracture toughness KIC by using the flattened Brazilian disk specimen for rocks. *Eng. Fract. Mech.* **1999**, *64*, 193–201. [CrossRef]
37. Hondros, G. The evaluation of Poisson's ratio and the modulus of materials of a low tensile resistance by the Brazilian (indirect tensile) test with particular reference to concrete. *Aust. J. Appl. Sci.* **1959**, *10*, 243–268.
38. Satoh, Y. Position and Load of Failure in Brazilian Test: A Numerical Analysis by Griffith Criterion. *J. Soc. Mater. Sci. Jpn.* **1987**, *36*, 1219–1224. [CrossRef]
39. Wang, F.; Xu, H.; Liu, Y.; Meng, X.; Liu, L. Mechanism of Low Chemical Agent Adsorption by High Pressure for Hydraulic Fracturing-Assisted Oil Displacement Technology: A Study of Molecular Dynamics Combined with Laboratory Experiments. *Langmuir* **2023**, *39*, 16628–16636. [CrossRef]
40. Xie, H.; Gao, F.; Ju, Y.; Fu, Q.; Zhou, F. Unconventional Theory and Technology Concept for Fracturing Modification of Shale Reservoirs. *J. Sichuan Univ. Eng. Sci. Ed.* **2012**, *44*, 1–6. [CrossRef]
41. Irwin, G.R. Analysis of Stresses and Strains Near End of a Crack Traversing a Plate. *J. Appl. Mech.* **1956**, *24*, 361–364. [CrossRef]
42. Zang, Z.; Li, Z.; Zhang, X.; Kong, X.; Gu, Z.; Yin, S.; Niu, Y. Electric potential response characteristics of coal under stress wave loading. *Nat. Resour. Res.* **2024**, *33*, 1289–1307. [CrossRef]
43. Lin, J.; Dong, C.; Lin, C.; Duan, D.; Ma, P.; Zhao, Z.; Liu, B.; Zhang, X.; Huang, X. The impact of tectonic inversion on diagenesis and reservoir quality of the Oligocene fluvial sandstones: The Upper Huagang Formation, Xihu Depression, East China Sea Shelf Basin. *Mar. Pet. Geol.* **2024**, *165*, 106860. [CrossRef]
44. Chong, K.P.; Kuruppu, M.D. New specimen for fracture toughness determination for rock and other materials. *Int. J. Fract.* **1984**, *26*, R59–R62. [CrossRef]
45. Chong, K.P.; Kuruppu, M.D.; Kuszmaul, J.S. Fracture toughness determination of layered materials. *Eng. Fract. Mech.* **1987**, *28*, 43–54. [CrossRef]
46. Zhang, J.; Lin, C.; Tang, H.; Wen, T.; Tannant, D.D.; Zhang, B. Input-parameter optimization using a SVR based ensemble model to predict landslide displacements in a reservoir area—A comparative study. *Appl. Soft Comput.* **2024**, *150*, 111107. [CrossRef]
47. Yao, J.; Ding, Y.; Sun, H.; Fan, D.; Wang, M.; Jia, C. Productivity Analysis of Fractured Horizontal Wells in Tight Gas Reservoirs Using a Gas–Water Two-Phase Flow Model with Consideration of a Threshold Pressure Gradient. *Energy Fuels* **2023**, *37*, 8190–8198. [CrossRef]
48. Kuruppu, M.D.; Obara, Y.; Ayatollahi, M.R.; Chong, K.P.; Funatsu, T. ISRM-suggested method for determining the mode I static fracture toughness using semi-circular bend specimen. *Rock Mech. Rock Eng.* **2014**, *47*, 267–274. [CrossRef]
49. ISRM. *The ISRM Suggested Methods for Rock Characterization, Testing and Monitoring*; Ulusay, R., Ed.; ISRM: Lisbon, Portugal, 2014; pp. 25–33.